

Cross-presentation of lactoferrin encapsulated into chitosan-based nanoparticles

Nanobiomedicine

Volume 3: 1–11

© The Author(s) 2016

Reprints and permissions:

sagepub.co.uk/journalsPermissions.nav

DOI: 10.1177/1849543516667355

nab.sagepub.com



Tatiana Lyalina¹, Anastasia Zubareva¹, Valery Varlamov¹,
and Elena Svirshchetskaya²

Abstract

Induction of CD8⁺ cytotoxic T-cell response is essential for the protection from intracellular pathogens. It requires major histocompatibility complex class I processing of newly synthesized proteins transported from the cytosolic pathway. Presentation of mature soluble proteins occurs via a cross-presentation (CP) pathway that is much less efficient in the activation of cytotoxic response. Encapsulation of proteins into polymeric nanoparticles (NPs) can modulate the efficacy of antigen CP. In this article, a model antigen lactoferrin (L) was encapsulated into polysaccharide NPs with different physicochemical properties (size, charge, and hydrophobicity) and used as an immunogen. CD8⁺ or CD4⁺ associated IgG2a or IgG1 subclasses of L-specific antibodies, respectively, served as a measure of CD8⁺ versus CD4⁺ T-cell activation. Among five types of NPs produced, only succinylchitosan–galactomannan (LSG) and succinylchitosan–PEG–chitosan (LSPC) NPs induced a significant IgG2a response. IgG1 production was comparable in all but hydrophobic succinyl-dodecyl-chitosan (LSD) NPs, where it was only marginal. Confocal studies demonstrated that galactomannan-equipped LSG-NPs induced vacuolar type of CP, while positively charged LSPC-NPs were transported mostly via the cytosolic CP pathway.

Keywords

Chitosan, nanoparticles, cross-presentation, mechanisms, lactoferrin

Date received: 15 May 2016; accepted: 11 August 2016

Introduction

A major goal in the development of effective vaccines against intracellular pathogens is the induction of a protective T-cell immunity mediated by CD8⁺ cytotoxic T cells. Modernly attenuated viral vaccines are used to elicit T-cell cytotoxic response in humans.¹ Protein vaccines could provide a complementary approach; however, they are poorly immunogenic for CD8⁺ cytotoxic T cells even when administered repeatedly in high doses. It is known that major histocompatibility complex (MHC) class I processing is the most efficient for newly synthesized viral proteins transported from the cytosolic pathway of infected antigen-presenting cells (APCs). Mature long-living endogenous and exogenous proteins are presented by APCs to CD8⁺ T cells

via a process called cross-presentation (CP). The mechanisms of CP are still a matter of debates.² Currently, “cytosolic” and “vacuolar” pathways are considered as the main

¹Enzyme engineering laboratory, Institute of Bioengineering, Research Center of Biotechnology of the Russian Academy of Sciences, Moscow, Russian Federation

²Immunology Department, Shemyakin–Ovchinnikov Institute of Bioorganic Chemistry of the Russian Academy of Sciences, Moscow, Russian Federation

Corresponding Author:

Elena Svirshchetskaya, Shemyakin–Ovchinnikov Institute of Bioorganic Chemistry of the Russian Academy of Sciences, Moscow, Russian Federation.
Email: esvir@mx.ibch.ru



Creative Commons CC-BY-NC: This article is distributed under the terms of the Creative Commons Attribution-Non Commercial 3.0 License (<http://www.creativecommons.org/licenses/by-nc/3.0/>) which permits non-commercial use, reproduction and distribution of the work without further permission provided the original work is attributed as specified on the SAGE and Open Access pages (<https://us.sagepub.com/en-us/nam/open-access-at-sage>).

models explaining how antigens can be processed to load MHC class I molecules for CP. In the cytosolic model, antigens are released from the endosomal compartment of APC to the cytoplasm where they are ubiquitinated and processed via proteosomal machinery like endogenous proteins.^{2,3} In the vacuolar model, antigens, degraded by endosomal or early lysosomal enzymes, are in situ loaded onto MHC I molecules. Fusion between the membrane of the endoplasmic reticulum and the endosome provides a source of MHC I molecules.⁴ It is generally accepted that the vacuolar form of CP occurs at high levels of antigen delivered into the endocytic pathway.

Analysis of antigen-specific CD4⁺ or CD8⁺ T cells is a complicated problem due to low number of these cells. Antigen-specific IgG1 and IgG2 serve as surrogate markers of their activation due to a direct dependence of B-cell switch to IgG1 or IgG2a on corresponding cytokines interleukin-4 and interferon- γ produced by APC during CD4⁺ or CD8⁺ T-cell activation.⁵⁻⁹

Encapsulation of proteins into polymeric nanocarriers enhances MHC I antigen presentation. Coupling of an antigen to beads mediated its delivery via the cytosolic pathway as was shown by Kovacsovics-Bankowski and Rock.¹⁰ Moreover, the structure of antigen carrier severely affects MHC I presentation. Antigen delivery by hyperbranched and cross-linked polymer nanoparticles (NPs) enhanced in vitro MHC I antigen presentation in comparison with linear constructs or free antigens.¹¹

Chitosan (C) is an attractive biopolymer with multiple reactive groups used to develop drug carries with different physicochemical properties such as charge, hydrophobicity, and particle size. Multiple reactive groups can be used to equip C NPs with targeting vectors. Folate-modified C NPs containing melanoma-associated antigen induced specific cytotoxic effect and inhibited tumor progression in mice.¹²

Among targeting vectors, Burgdorf et al. showed that mannose receptor ligands promote the formation of cytotoxic response due to the prevention of lysosome maturation.¹³ Mannose receptor–dependent antigen CP of soluble proteins occurred in early endosomes, which is consistent with the vacuolar hypothesis.¹³ Mannosylation of peptides enhances CP as was shown by Rauen et al.¹⁴ The effect of mannose receptor targeting vectors on the cytotoxic immune response induced by encapsulated antigens was not previously shown.

The role of NP surface charge in hydrophilic/hydrophobic properties in CP is not well understood. Negatively charged poly(lactid-co-glycolid) NPs were transported to lysosomal compartment and effectively induced cytotoxic response.¹⁵ At the same time, amino group–modified but not carboxyl-modified polystyrene NPs were found in lysosomes.¹⁶ Hydrophilic poly(lactide-co-hydroxymethylglycolic acid) NPs were effective in the CD8⁺ cytotoxic response induction to a model antigen.¹⁷ The data on the CP of antigens delivered by hydrophobic NPs are lacking.

The aim of this article was to compare CP efficacy of a model antigen lactoferrin (L) encapsulated into NPs with different physicochemical properties. The role of charge, hydrophobicity, and mannose receptor vector was considered.

Materials

Chitosan (C) with molecular weight (MW) 20 kDa and deacetylation degree (DD) 90% and succinylchitosan (S) obtained from C with MW 50 kDa and DD 70% (ZAO “Bioprogress,” Moscow region, Russian Federation) were purified by extensive dialysis. Lactoferrin (L), galactomannan (G), and polyethylene glycol 2000 kDa (Sigma-Aldrich, St. Louis, MO, USA) were used as purchased. *N*-[2-(3)-(dodec-2'-en-1'-yl)succinyl]chitosan (SD) was synthesized as described earlier¹⁸ from 50 kDa C.

Methods

Formation of NPs

Core NPs were prepared by controlled thermal treatment of either pure L 1 mg/ml solution (L-NPs); or weight 1:1 ratio mixtures of L, S, and polyethyleneglycol (PEG) (LSP-NPs); L, S, and G (LSG-NPs); or L and SD. L or L-polymer mixtures were rapidly heated to 85–90°C and incubated for 5–10 min. Core-shell LSPC-NPs were prepared from LSP-NPs resuspended in 10 mg/ml of C solution and incubated for 15 min. NPs were separated from free L and polymers by centrifugation for 15 min at 14,000 r/min. NPs were resuspended in 50 mM phosphate-buffered saline (PBS) of pH 7.4. L content was around 10%. For confocal and flow cytometry experiments, L was labeled with fluorescein isothiocyanate (FITC) (Sigma-Aldrich) and used to form NPs.

Dynamic light scattering

The diameter of NPs was characterized by dynamic light scattering (90 Plus Particle Size Analyzer; Brookhaven Instruments Corporation, Vernon Hills, Illinois, USA). All measurements were performed using a 661-nm laser light at room temperature with a 90° angle of detection. The zeta potential of χ was determined in 10 mM potassium chloride using identical equipment with an additional ZetaPALS apparatus.

Atomic force microscopy

Particle size and morphology were measured by atomic force microscopy (AFM) on NTEGRA Prima microscope (NT-MDT, Russia) in tapping mode with the use of NSG01 cantilevers. The preliminary sample was placed on a mica surface and air dried.

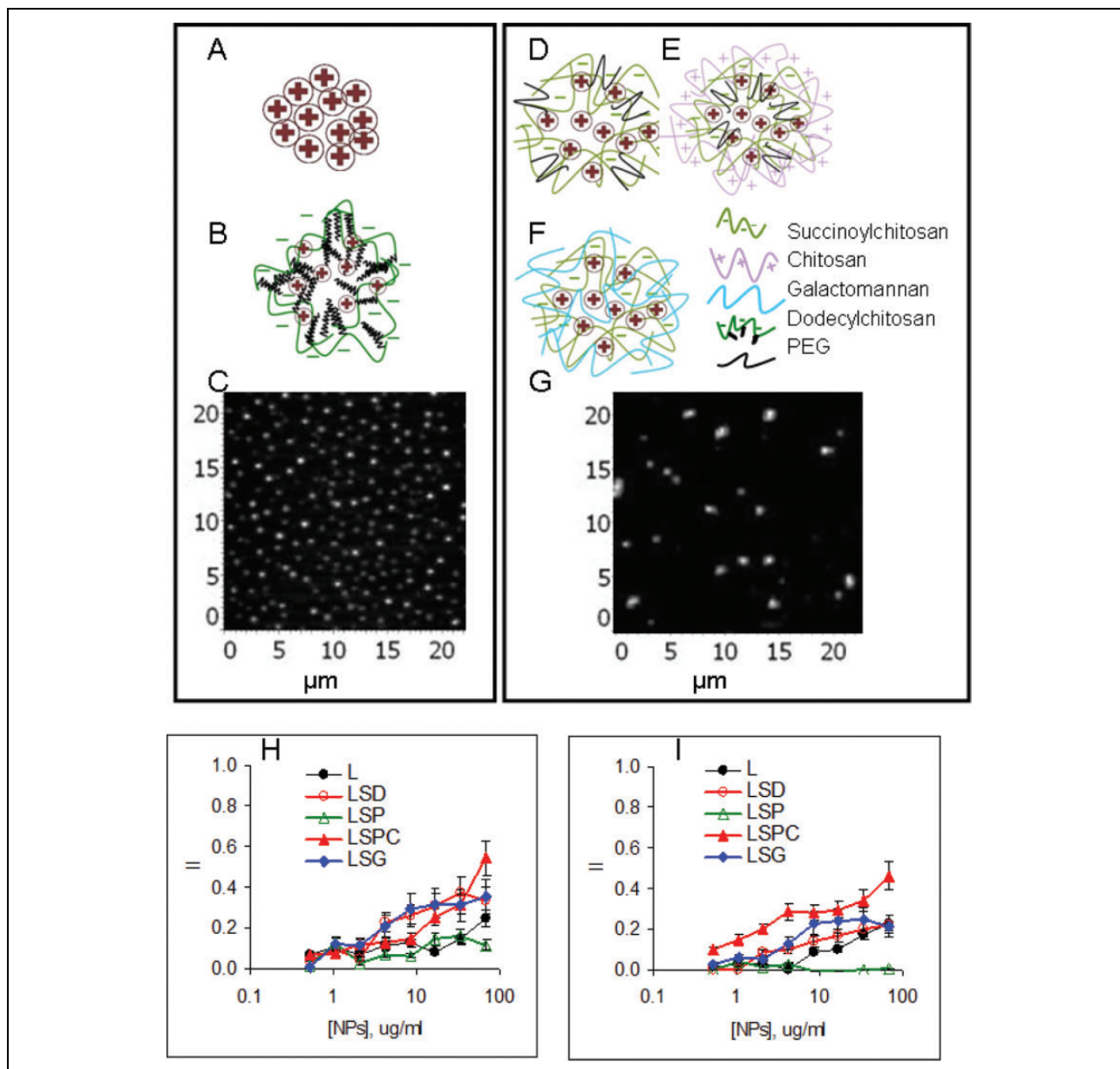


Figure 1. Characterization of nanoparticles. Schematic structure of small (110–140 nm) L-NPs (a), LSD-NPs (b), large (300–420 nm) LSP-NPs (d), LSPC-NPs: LSP-NPs nanoparticles additionally coated by chitosan; (e), and LSG-NPs (f); AFM images of small (c) and large (g) NPs; cytotoxicity of NPs against tumor Colo-357 (h) and control HEK293 (i) cell lines. L-NPs: lactoferrin-nanoparticles; LSD-NPs: nanoparticles from lactoferrin mixed with dodecylsuccinyl-chitosan; LSP-NPs: nanoparticles from lactoferrin mixed with succinyl-chitosan and PEG2000; LSG-NPs: nanoparticles from lactoferrin mixed with succinyl-chitosan and galactomannan; LSPC-NPs: nanoparticles from lactoferrin mixed with succinyl-chitosan and PEG2000 and additionally coated with chitosan; AFM: atomic force microscopy. (See Table 1 for the abbreviations).

Table 1. Characterization of nanoparticles.

#	Designation	Antigen	Polymer	ζ -potential (mV)	Size (nm)
1	L-NPs	Lactoferrin	None	+22 ± 3	110–130
2	LSD-NPs	Lactoferrin	Dodecylsuccinylchitosan	-14 ± 3	120–140
3	LSP-NPs	Lactoferrin	Succinylchitosan-PEG	-16 ± 5	300–400
4	LSPC-NPs	Lactoferrin	(Succinylchitosan-PEG)chitosan	+19 ± 4	350–420
5	LSG-NPs	Lactoferrin	Succinylchitosan-galactomannan	-15 ± 4	300–350

L-NPs: lactoferrin-nanoparticles; LSD-NPs: nanoparticles from lactoferrin mixed with dodecylsuccinyl-chitosan; LSP-NPs: nanoparticles from lactoferrin mixed with PEG2000; LSG-NPs: nanoparticles from lactoferrin mixed with galactomannan.

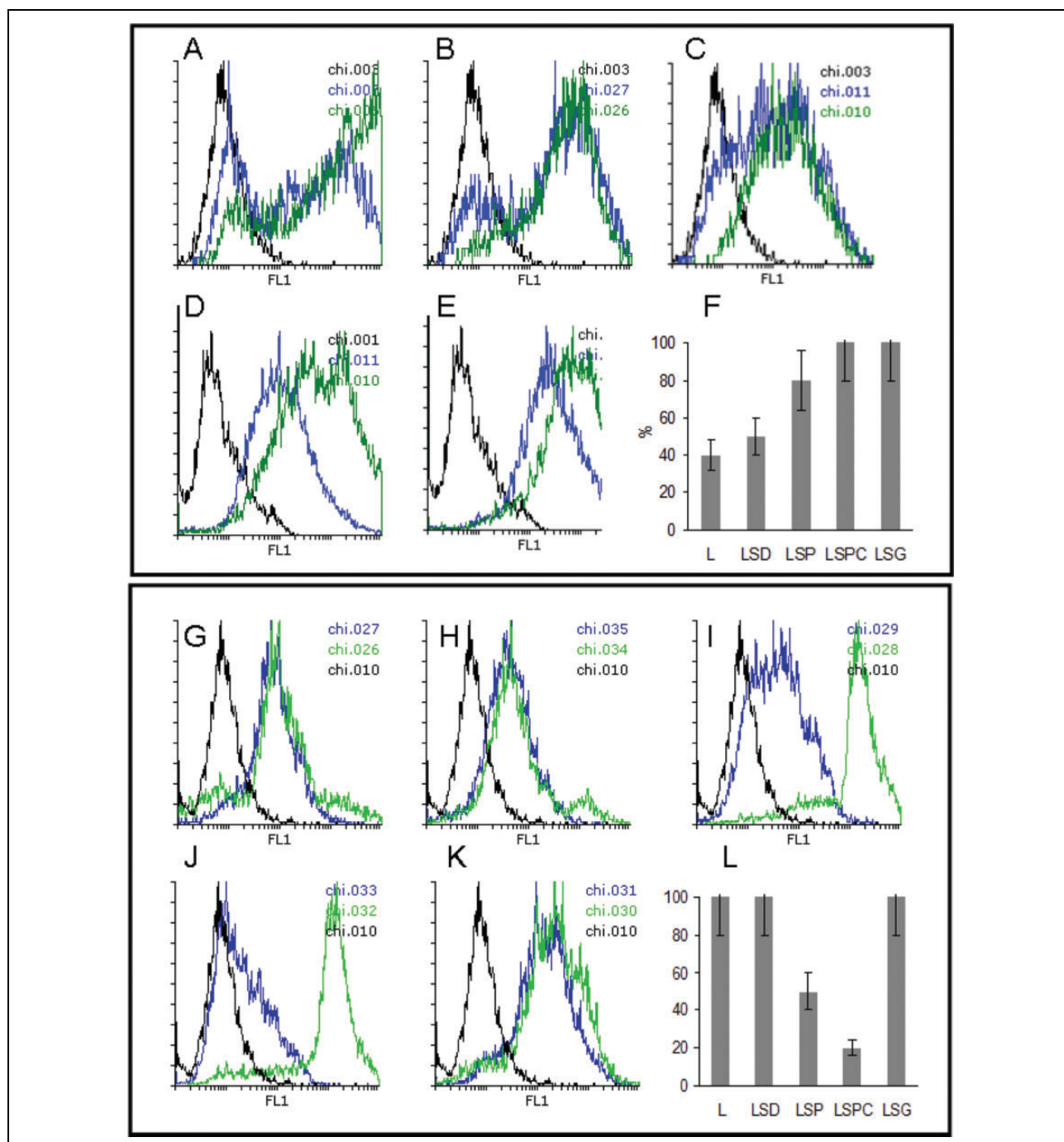


Figure 2. In vitro NP binding to and penetration into macrophage and epithelial cells. Control cells are shown in black lines; NP bound to cells are shown by green lines, and intracellular NPs were identified after trypan blue quenching and shown in blue lines. Binding and penetration of L-NPs (a and g), LSD-NPs (b and h), LSP-NPs (c and i), LSPC-NPs (d and j), and LSG-NPs (e and k) into RAW264.7 (a to f) and Colo-357 (g to l). Summary results on intracellular localization of NPs in RAW264.7 (f) and Colo-357 (l). (See Figure 1 legend and Table 1 for the abbreviations).

Cell lines

Human pancreatic carcinoma Colo-357, fetal human kidney HEK-293, and murine macrophage RAW264.7 cell lines were grown in Dulbecco's modified Eagle medium supplemented with 7% fetal calf serum (HyClone, New

Kensington, PA, USA), pen-strep-glut, and 2 mercaptoethanol (2-ME) 5×10^{-5} M (all from PanEco, Moscow, Russian Federation). Cells were passaged by trypsinization using trypsin/ethylenediaminetetraacetic acid solution (PanEco) twice a week. Twenty-four hours before assays, cells were seeded in the appropriate plates

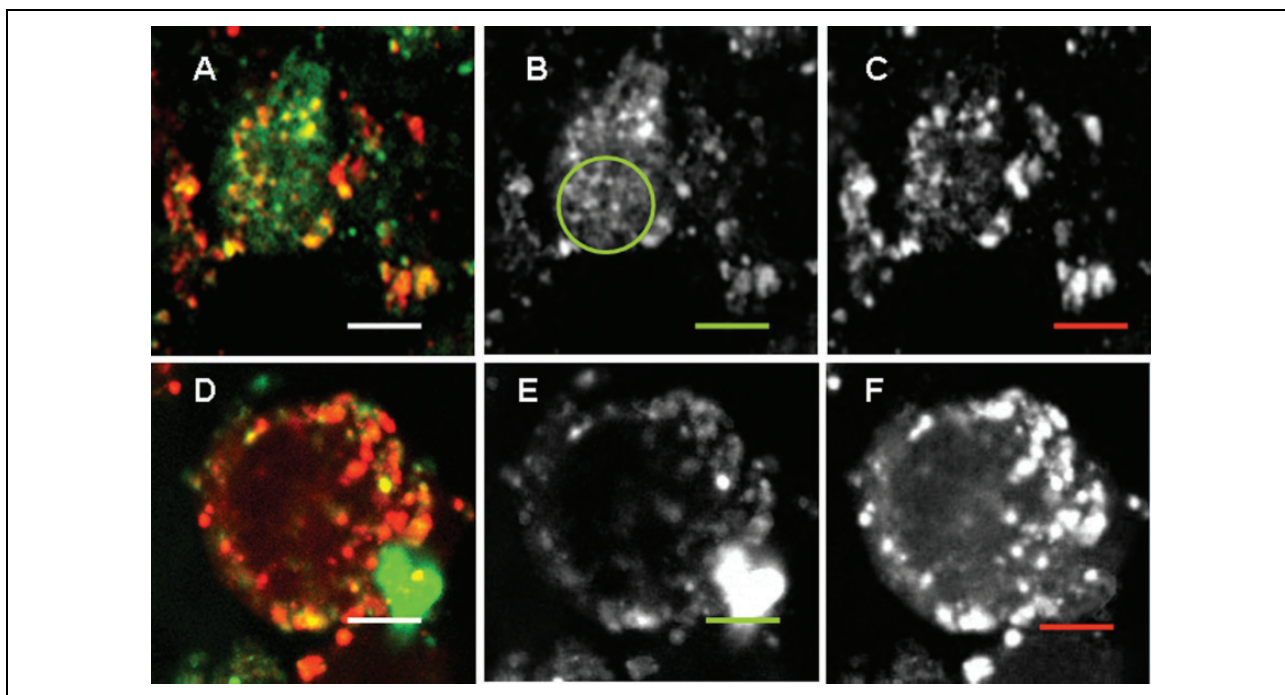


Figure 3. Colocalization of positively charged NPs with lysosomes. RAW264.7 cells were incubated with 50 $\mu\text{g/ml}$ of FITC-labeled L-NPs (a to c) or LSPC-NPs (d to f) (green) for 24 h; LyzoTrackerRed was added for the last hour. Overlaid, green and red images are shown from left to right. Scale bar corresponds to 5 μm . Noncoinciding staining is shown with a circle. (See Figure 1 legend and Table 1 for the abbreviations).

(96- or 24-well plates) adjusted to 3×10^5 cells per milliliter and incubated overnight to achieve standardized growth conditions.

Confocal microscopy

For confocal microscopy, cells were grown overnight on sterile cover slips in 200 μl of a complete culture medium in 6-well plates (CoStar, Cambridge, MA, USA). NPs (50 $\mu\text{g/ml}$) were added and incubated with the cells for 24 h. Hoechst 33342 (Sigma-Aldrich), MitoTracker[®] Red, LysoTracker[®] Red DND-99, human transferrin-Alexa Fluor[®] 568 Conjugate, and Wheat Germ Agglutinin-Alexa Fluor[®] 555 Conjugate (all from Life Technologies, Waltham, MA, USA) used to localize NPs inside cells were added for the last 1 h of incubation. Before the analysis, extracellular FITC fluorescence was quenched with Trypan blue solution (0.1%) for 10 min as described earlier.¹⁹ After that, cells were washed with a fresh medium, fixed with 1% paraformaldehyde, washed, and polymerized with Mowiol 4.88 medium (Calbiochem, Germany). Slides were analyzed using an Eclipse TE2000 confocal microscope (Nikon, Japan).

MTT assay

The cytotoxic effect of NPs was estimated by a standard 3-(4,5-dimethyl-2-thiazolyl)-2,5-diphenyl-2H-tetrazolium bromide

(MTT; Sigma-Aldrich) test as was described earlier.²⁰ The inhibitory index (II) was calculated as $\text{II} = [1 - (\text{OD}_{\text{experiment}}/\text{OD}_{\text{control}})]$, where OD is the MTT optical density.

Flow cytometry

NP binding to cells was estimated by flow cytometry. NP samples (50 $\mu\text{g/ml}$) were incubated with the cells for 24 h, trypsinized, and analyzed by flow cytometry using a FACScan device (BD, San Jose, CA, USA). Before the analysis, extracellular FITC fluorescence was quenched with Trypan blue solution (0.1%) for 10 min. A total of 10,000 events were collected. The results were analyzed using Flowing software.

Experiments in vivo

C57Bl/6 mice (8 weeks of age) were purchased from Pushchino Farm (Moscow Region, Russian Federation) and kept at minimum disease conditions. Mice ($n = 4$) were immunized subcutaneously in hind paw with 10 μg per mouse of L equivalent three times with a 5-day interval. Sera were collected 2 weeks after the last immunization.

Enzyme-linked immunosorbent assay

Levels of L-specific serum IgG, IgG1, and IgG2a were measured as elsewhere described. L (10 $\mu\text{g/mL}$) in PBS was

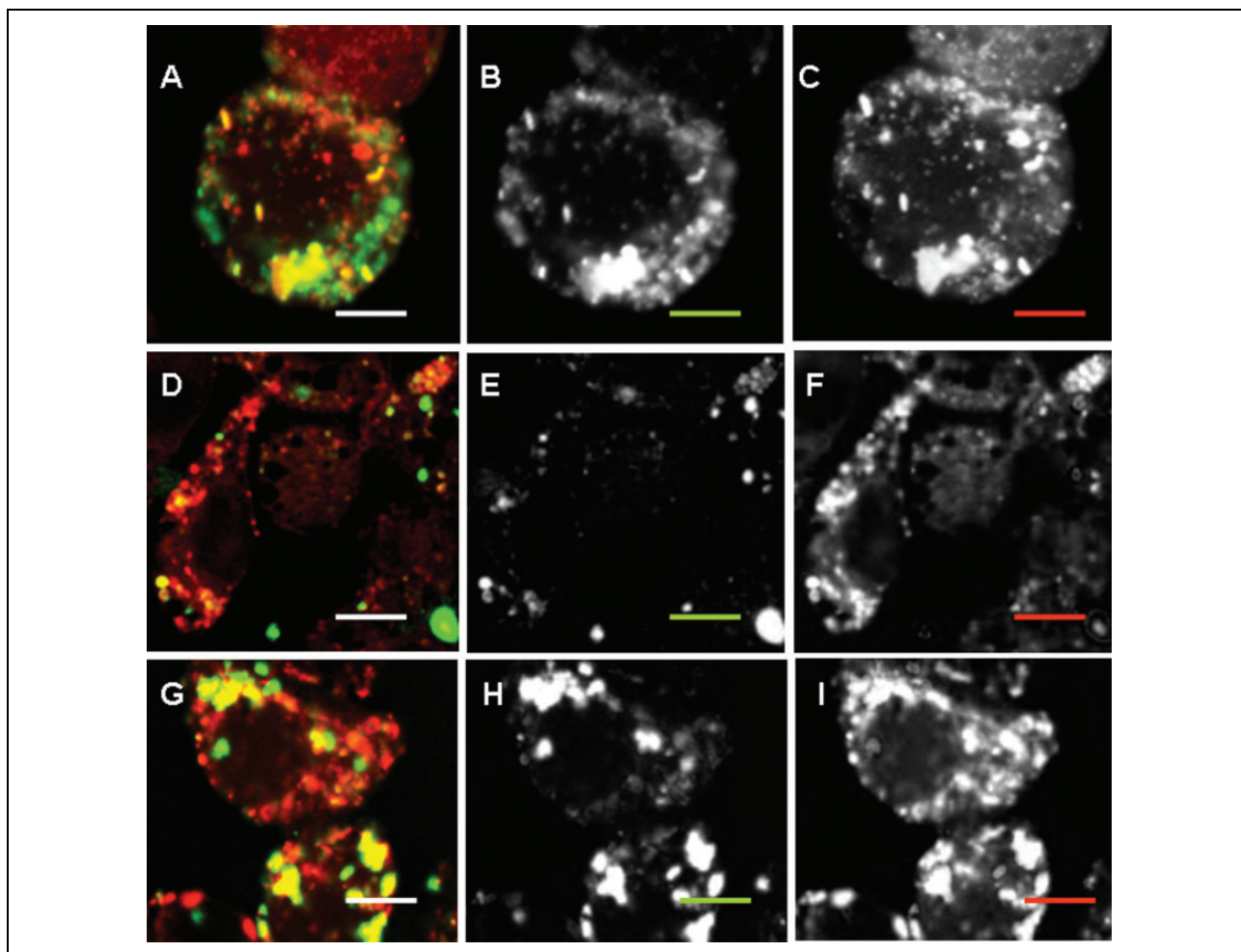


Figure 4. Colocalization of negatively charged NPs with lysosomes. RAW264.7 cells were incubated with 50 $\mu\text{g}/\text{ml}$ of FITC-labeled LS-NPs (a to c), LSG-NPs (d to f), or LSD-NPs (g to i) (green) for 24 h; LyzoTrackerRed was added for the last hour. Overlaid, green and red images are shown from left to right. Scale bar corresponds to 5 μm . (See Figure 1 legend and Table 1 for the abbreviations).

coated onto microtiter plates and kept at 4°C overnight. Plates were washed three times with PBS containing 0.05% Tween 20 between each step. Unspecific binding was blocked with 10% of bovine albumin. Antimouse conjugate of immunoglobulin G (IgG-HRP) (Sigma-Aldrich), conjugates of immunoglobulin G1 or G2a with alkaline phosphatase (IgG1-AP, and IgG2a-AP) (SantaCruz, CA, USA) were used at the dilutions recommended by the firm. The mean plus 3 standard deviations of absorbance values in control wells was used as the cutoff to determine immunoglobulins (Ig) titers. The results are shown as Ig titers that were determined as the last serum dilution above cutoff values.

Statistics

Statistical analysis was performed using Student's *t*-test. Comparison values of $p < 0.05$ were considered statistically significant.

Results and discussion

Characterization of antigen-loaded NPs

The main idea was to encapsulate a model antigen L into a polymeric matrix with a difference in surface charge and hydrophobicity or equipped it with a mannose receptor ligand G (Figure 1 (a) to (f)). L was selected as a model antigen due to its ability to bind L receptors expressed by tumor cells.²¹ Besides, due to a globular structure of L, stable NPs can be formed by a simple method that does not require chemical conjugation.²² L to polymer ratio was optimized by titration of polymer against L to obtain high protein content. Finally, 1:1 w/w L/polymer ratio was selected, which provided approximately 50% protein content in all NPs developed. The yield of NPs from L mixed with succinylchitosan (LS-NPs) was low and inclusion of PEG2000 (LSP-NPs) or galactomannan (LSG-NPs) significantly increased it. L

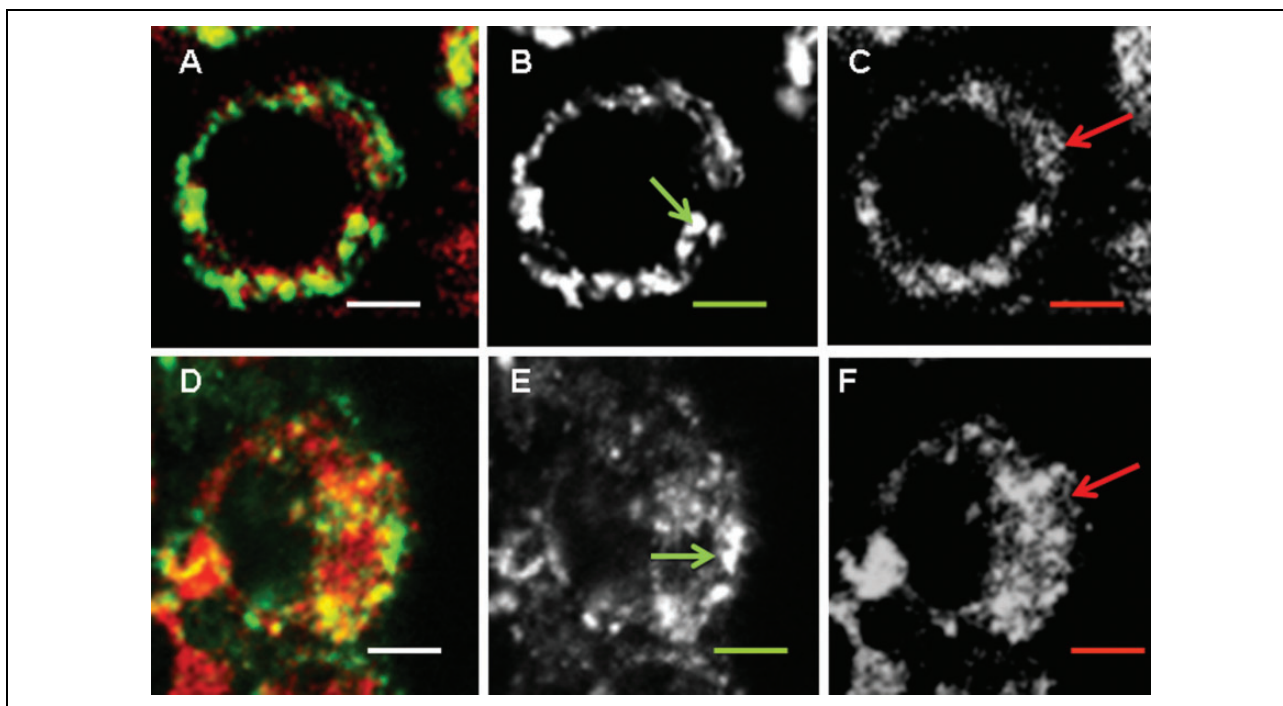


Figure 5. Colocalization of positively charged NPs with endoplasmic reticulum. RAW264.7 cells were incubated with 50 $\mu\text{g/ml}$ of FITC-labelled L-NPs (a to c) or LSPC-NPs (d to f) (green) for 24 h; endoplasmic reticulum (EPR) tracker was added for the last hour. Overlaid, green and red images are shown from left to right. Scale bar corresponds to 5 μm . Vesicular structures are shown with green arrow, EPR cisternae structures are shown with red arrows. (See Figure 1 legend and Table 1 for the abbreviations).

with hydrophobic C derivative dodecylsuccinylchitosan (LSD-NPs) formed compact stable NPs with a high yield. Four of five NPs were developed in a single-step procedure. Positively charged LSPC-NPs were obtained by polyelectrolyte complex formation between LSP-NPs and C. The final NPs were dissolved in water at 500 $\mu\text{g/ml}$ of L. The main characteristics of all NPs are shown in Table 1. Representative images of small and large NPs obtained by AFM are shown for L-NPs (Figure 1(c)) and LSP-NPs (Figure 1(g)).

Cytotoxicity of L-based NPs was estimated by MTT assay using tumor (Colo-357) and control (HEK-293) epithelial cell lines. On average, cytotoxicity was comparable between cell lines (Figure 1(h) and (i)) and decreased in a row: LSPC-NPs > LSD-NPs > LSGNPs > L-NPs > LSP-NPs. Of note, positively and negatively charged NPs were opposite in their toxicity, which is in line with many other observations.^{23,24}

In vitro interaction of L-based NPs with cells

L-based NPs were designed to deliver the antigen to the immune cells for CP, which takes place in APC. Thus, it was essential to analyze the interaction of NPs with phagocytic cells. Epithelial cells were included as a control. Preliminary experiments showed that NPs effectively bound cells within minutes; however, a significant amount

of particles were localized on cell membranes as was estimated using Trypan blue quenching¹⁹ (data not shown). Coincubation for 24 h resulted in a complete phagocytosis of LSPC-NPs and LSG-NPs but not of other NPs by RAW264.7 murine macrophages (Figure 2(a)–(f)). Contrary to macrophages, an inverse situation was found for the epithelial cells that completely absorbed L-NPs and LSD-NPs but not LSP-NPs or LSPC-NPs (Figure 2(g) to (l)). LSG-NPs equipped with a mannose receptor ligand G penetrated effectively both macrophage and epithelial cells presumably via a receptor-mediated uptake. Expression of mannose receptor by epithelial cells and especially by tumor epithelial cells was shown earlier.^{25,26} High LSP-NPs and LSPC-NP uptake by macrophages can be explained by their phagocytic activity, which epithelial cells lack. High L-NPs uptake by epithelial cells probably occurs via L receptor binding,²⁷ while LSD-NP penetration into epithelial but not macrophage-like cells is likely a result of mucoadhesive properties of hydrophobic C that is able to bind mucin.²⁸

Traffic of polymeric NPs via endosomal/lysosomal pathway

Localization of NPs in endosomal/lysosomal compartment corresponds to a classical transport of exogenous and even

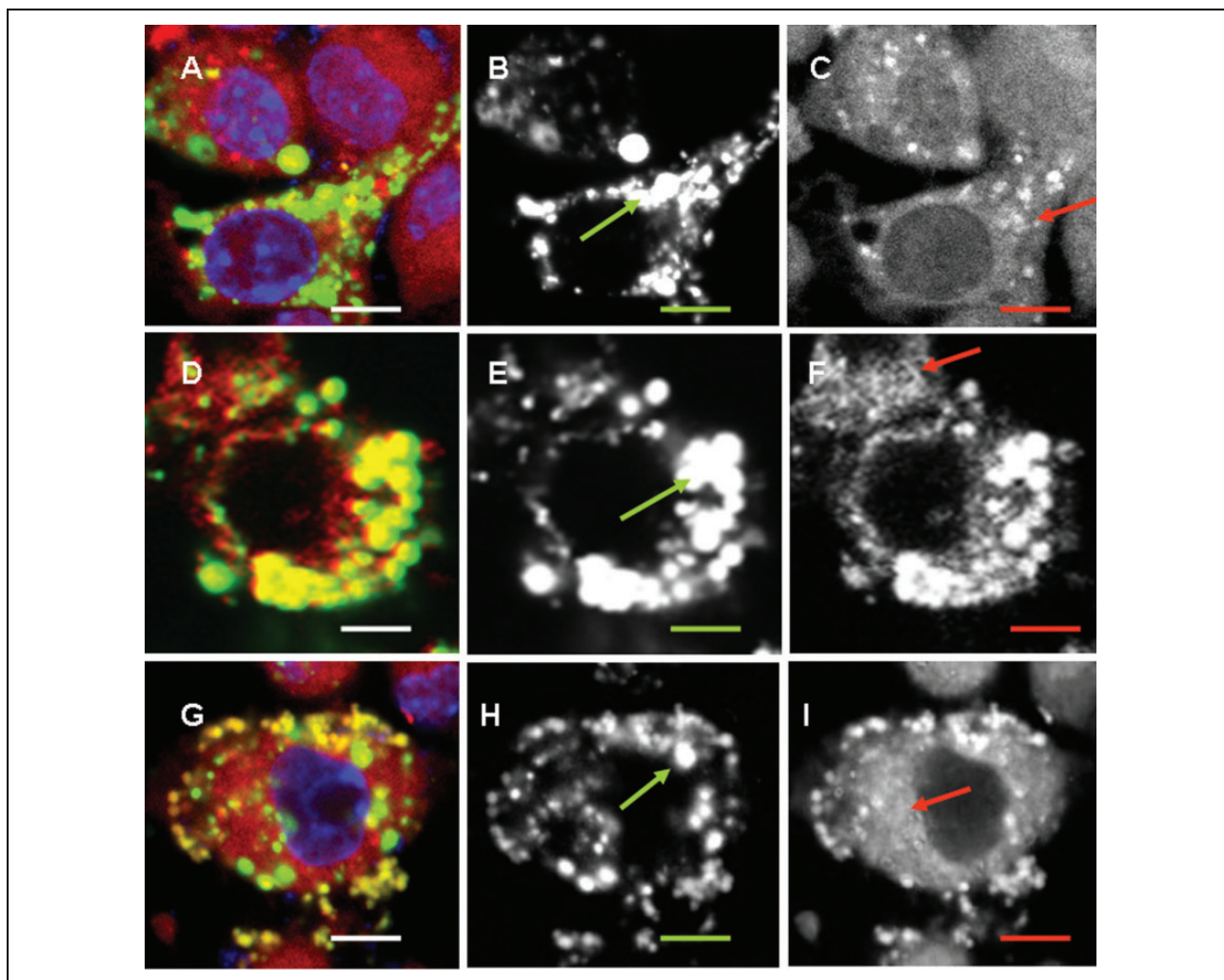


Figure 6. Colocalization of negatively charged NPs with endoplasmic reticulum. RAW264.7 cells were incubated with 50 $\mu\text{g/ml}$ of FITC-labeled LS-NPs (a to c), LSG-NPs (d to f), or LSD-NPs (g to i) (green) for 24 h; EPR tracker was added for the last hour. Overlaid, green and red images are shown from left to right. Scale bar corresponds to 5 μm . Vesicular structures are shown with green arrow and EPR cisternae structures are shown with red arrows. (See Figure 1 legend and Table 1 for the abbreviations).

endogenous mature long-living proteins, which results in humoral IgG1-dominated immunity. Localization of positively charged L-NPs and CSPC-NPs slightly differed. A significant amount of L-NPs did not colocalize with the lysosomal tracker (Figure 3(b) shown with a green circle), while CSPC-NPs were found mostly in endosomal vesicles (Figure 3). All negatively charged NPs were found in lysosomes (Figure 4).

Colocalization of NPs with endoplasmic reticulum (EPR)

Colocalization with EPR means that either MHC I molecules associated with the fragments of EPR membranes are fused to endosomes or that large fragments on NPs are transported directly to EPR. Despite partial overlap of

different light colors, EPR and endosomes/lysosomes could be distinguished by different morphology. EPR represents a cisternae membrane network (Figure 5, red arrows), while lysosomes are spherical vesicles (Figure 5, green arrows). Positively charged L-NPs and LSPC-NPs were found both in vesicles and among EPR network (Figure 5), while all negatively charged NPs were predominately found in vesicular compartments (Figure 6). Among three types of negatively charged NPs, those that contain G induced the deposition of EPR fragments into vesicles most efficiently (Figure 6(d) to (f)), while LSP-NPs were the least effective (Figure 6(a) to (c)). Earlier effect of G on CP was shown.^{13,14} Hydrophobic LSD-NPs were also found within the vesicular compartment; however, their location seemed to be outside of the cells (Figure 6(g) to (i)), probably due to exocytosis of lysosomes.

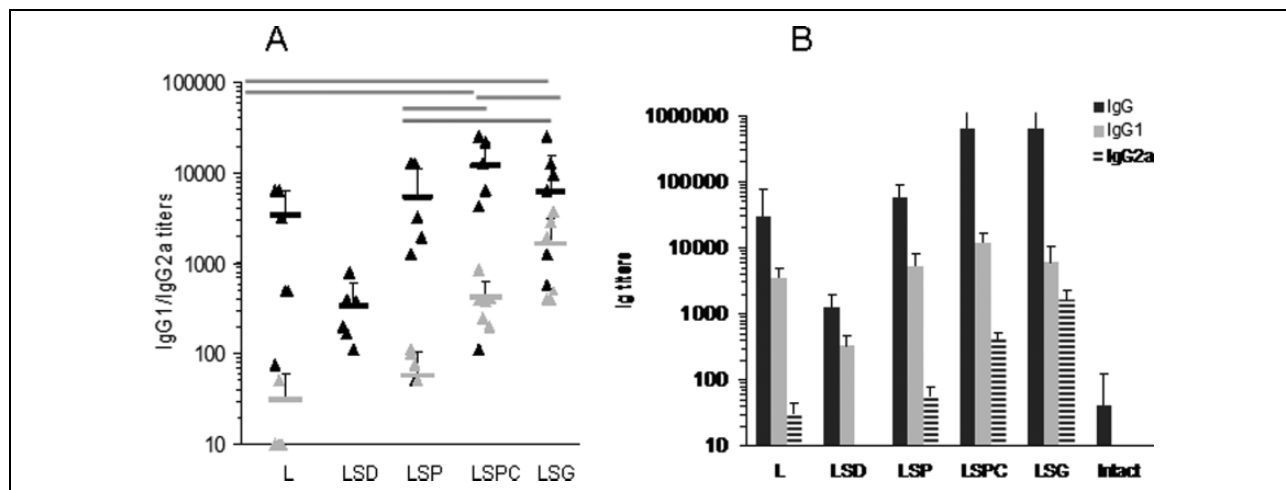


Figure 7. Distribution of immunoglobulins specific to lactoferrin. (a) IgG1 (black) and IgG2a (gray) titers in individual mice immunized with different NPs. Statistical difference ($p < 0.05$) shown in gray bars was found only in IgG2a, but not IgG1 for the exception for LSD-NPs, which induced lower IgG1 titers (shown with asterisk). (b) Average titers of IgG (stripped), IgG1 (black), and IgG2a (gray). (See Figure 1 legend and Table 1 for the abbreviations).

In vivo effect of L-based NPs

Mice were immunized with 10 μg per mouse of L equivalent three times with a 5-day interval. Sera were collected 2 weeks after the last immunization. IgG1 and IgG2a titers of individual mice are shown in Figure 7(a). The lowest immunogenicity was found for hydrophobic LSD-NPs, which only slightly increased L-specific IgG1 production. Among others, NPs IgG1 production was comparable ($p > 0.05$), while IgG2a titers increased in a row: L-NPs < LSP-NPs < LSPC-NPs < LSG-NPs. A direct correlation was found between NP penetration into RAW264.7 cells (Figure 2(a) to (f)) and IgG2a response (Figure 7) ($p < 0.05$). The only exception was hydrophobic LSD-NPs that were unable to mount IgG2a response and induced only low titers of IgG1. It can be hypothesized that hydrophobic NPs were retained by epithelial cells preventing efficient entrapment by APC.

As expected, the titers of IgG1 were 3–10 times higher than that of IgG2a, meaning that STAT6 transcription factor was activated and mostly Th2 cytokines were produced.²⁹ However, IgG2a production associated with STAT1 activation and interferon gamma synthesis³⁰ was also found in mice immunized with LSP-, LSPC-, or LSG-NPs. Of note, L was shown to preferentially mount IgA and IgG2b responses in mice.³¹

Modernly, CP is thought to occur through two main pathways: by endosomal processing where antigen is degraded by the enzymes into peptides that bind to MHC I molecules within the endocytic pathway or by cytosolic processing where the antigen is delivered into cytosol by unknown mechanisms and degraded by proteasomes. Despite intensive research, the mechanisms of the latter process are mostly speculative.³²

Earlier, we have shown that positively charged C and C-based NPs poorly penetrated epithelial cells and were

engulfed mostly by macrophages.³³ At the same time, negatively charged succinylchitosan and corresponding NPs easily penetrated all types of cells and were transported into lysosomal compartment. Based on our earlier results and the results obtained in this study, it can be hypothesized that CP via cytosolic pathway is effective for positively charged molecules. Cell membranes are negatively charged. Positive charge of NPs is likely to interfere with the capacitance of the membrane barrier in cells leading to their shedding into extracellular space as it was found for LSD-NPs (Figure 6(g) to (i)). During this process, some amount of positively charged material may have excess into cytosol of cells. Interaction of positively charged polymers with negatively charged cell membrane is likely to induce membrane shedding. During this process, some amount of positively charged material may have excess into cytosol of cells.

Conclusions

Taken collectively, encapsulation of antigens into polymeric matrix can significantly change the traffic of proteins within APC and affect both humoral and cellular immune responses. Decorating NPs with mannose receptor ligand results in increased CP via vacuolar pathway, while positively charged polymers facilitate cytosolic pathway. When comparing the effect of vacuolar and cytosolic CP, G-mediated fusion of EPR membranes with endosomal vesicles seems to be more efficient.

Declaration of conflicting interests

The author(s) declared no potential conflicts of interest with respect to the research, authorship, and/or publication of this article.

Funding

The author(s) disclosed receipt of the following financial support for the research, authorship, and/or publication of this article: The research was supported by the Russian Scientific Foundation, grant no. 16-14-00046, and Russian Federation President Scholarships donated to A A Zubareva (no. 1386.2015.4).

References

- Plotkin SA. Vaccines: the fourth century. *Clin Vaccine Immunol* 2009; 16: 1709–1719. DOI: 10.1128/CVI.00290-09.
- Norbury CC. Defining cross presentation for a wider audience. *Curr Opin Immunol* 2016; 40: 110–116. DOI: 10.1016/j.coi.2016.04.003.
- Gutiérrez-Martínez E, Planès R, Anselmi G, et al. Cross-presentation of cell-associated antigens by MHC class I in dendritic cell subsets. *Front Immunol* 2015; 6: 363. DOI: 10.3389/fimmu.2015.00363.
- Gagnon E, Duclos S, Rondeau C, et al. Endoplasmic reticulum-mediated phagocytosis is a mechanism of entry into macrophages. *Cell* 2002; 110(1): 119–131. DOI: 10.1016/S0092-8674(02)00797-3.
- Stavnezer J. Immunoglobulin class switching. *Curr Opin Immunol* 1996; 8: 199–205.
- Manis JP, Tian M and Alt FW. Mechanism and control of class-switch recombination. *Trends Immunol* 2002; 23: 31–39.
- Xu W and Zhang JJ. Stat1-dependent synergistic activation of T-bet for IgG2a production during early stage of B cell activation. *J Immunol* 2005; 175(11): 7419–7424.
- Takeda K, Tanaka T and Shi W. Essential role of Stat6 in IL-4 signaling. *Nature* 1996; 380: 627–630.
- Swaminathan G, Thoryk EA, Cox KS, et al. A novel lipid nanoparticle adjuvant significantly enhances B cell and T cell responses to sub-unit vaccine antigens. *Vaccine* 2016; 34(1): 110–119.
- Kovacsóvics-Bankowski M and Rock KL. A phagosome-to-cytosol pathway for exogenous antigens presented on MHC class I molecules. *Science* 1995; 267(5195): 243–246. DOI: 10.1126/science.7809629.
- Wilson JT, Postma A, Keller S, et al. Enhancement of MHC-I antigen presentation via architectural control of pH-responsive, endosomolytic polymer nanoparticles. *AAPS J* 2015; 17(2): 358–369. DOI: 10.1208/s12248-014-9697-1.
- He J, Duan S, Yu X, et al. Folate-modified Chitosan nanoparticles containing the IP-10 gene enhance melanoma-specific cytotoxic CD8(+) CD28(+) T lymphocyte responses. *Theranostics* 2016; 6(5): 752–761. DOI: 10.7150/thno.14527.
- Burgdorf S, Kautz A, Bohnert V, et al. Distinct pathways of antigen uptake and intracellular routing in CD4 and CD8 T cell activation. *Science* 2007; 316(5824): 612–616. DOI: 10.1126/science.1137971.
- Rauen J, Kreer C, Paillard A, et al. Enhanced cross-presentation and improved CD8+ T cell responses after mannosylation of synthetic long peptides in mice. *PLoS One* 2014; 9(8): e103755. DOI: 10.1371/journal.pone.0103755.
- Costa Lima SA, Silvestre R, Barros D, et al. Crucial CD8(+) T-lymphocyte cytotoxic role in amphotericin B nanospheres efficacy against experimental visceral leishmaniasis. *Nano-medicine* 2014; 10(5): 1021–1030. DOI: 10.1016/j.nano.2013.12.013.
- Ekkapongpisit M, Giovia A, Follo C, et al. Biocompatibility, endocytosis, and intracellular trafficking of mesoporous silica and polystyrene nanoparticles in ovarian cancer cells: effects of size and surface charge groups. *Int J Nanomed* 2012; 7: 4147–4158. DOI: 10.2147/IJN.S33803.
- Rahimian S, Kleinovink JW, Franssen MF, et al. Near-infrared labeled, ovalbumin loaded polymeric nanoparticles based on a hydrophilic polyester as model vaccine: in vivo tracking and evaluation of antigen-specific CD8(+) T cell immune response. *Biomaterials* 2015; 37: 469–477. DOI: 10.1016/j.biomaterials.2014.10.043.
- Tikhonov VE, Stepnova EA, Babak VG, et al. Amphiphilic N-[2(3)-(dodec-2'-en-1'-yl)succinoyl]chitosan: synthesis and properties. *React Funct Polym* 2008; 68(2): 436–445. DOI: 10.1016/j.reactfunctpolym.2007.11.002.
- Santos EO, Azzolini AE and Lucisano-Valim YM. Optimization of a flow cytometric assay to evaluate the human neutrophil ability to phagocytose immune complexes via Fcγ and complement receptors. *J Pharmacol Toxicol Methods* 2015; 72: 67–71. DOI: 10.1016/j.vascn.2014.10.005.
- Mosmann T. Rapid colorimetric assay for cellular growth and survival: application to proliferation and cytotoxicity assays. *J Immunol Methods* 1983; 65(1-2): 55–63. DOI: 10.1016/0022-1759(83)90303-4.
- Mehra NK, Mishra V and Jain NK. Receptor-based targeting of therapeutics. *Ther Deliv* 2013; 4(3): 369–94. DOI: 10.4155/tde.13.6.
- Il'ina AV, Kurek DV, Zubareva AA, et al. Preparation and characterization of biopolymer nanoparticles based on lactoferrin-polysaccharide complexes. *React Funct Polym* 2016; 102: 33–38. DOI: 10.1016/j.reactfunctpolym.2016.03.003.
- Kim CS, Nguyen HD, Ignacio RM, et al. Immunotoxicity of zinc oxide nanoparticles with different size and electrostatic charge. *Int J Nanomed* 2014; 9(Suppl 2): 195–205. DOI: 10.2147/IJN.S57935.
- Fröhlich E. The role of surface charge in cellular uptake and cytotoxicity of medical nanoparticles. *Int J Nanomed* 2012; 7: 5577–5591. DOI: 10.2147/IJN.S36111.
- Wang Q, Zhao G, Lin J, et al. Role of the mannose receptor during aspergillus fumigatus infection and interaction with dectin-1 in corneal epithelial cells. *Cornea* 2016; 35(2): 267–273. DOI: 10.1097/ico.0000000000000710.
- Liu Z, Ke F, Duan C, et al. Mannan-conjugated adenovirus enhanced gene therapy effects on murine hepatocellular carcinoma cells in vitro and in vivo. *Bioconjug Chem* 2013; 24(8): 1387–1397. DOI: 10.1021/bc400215a.
- Jiang R, Lopez V, Kelleher SL, et al. Apo- and holo-lactoferrin are both internalized by lactoferrin receptor via clathrin-mediated endocytosis but differentially affect

- ERK-signaling and cell proliferation in Caco-2 cells. *J Cell Physiol* 2011; 226(11): 3022–3031. DOI: 10.1002/jcp.22650.
28. Menchicchi B, Fuenzalida JP, Bobbili KB, et al. Structure of chitosan determines its interactions with mucin. *Bio-macromolecules* 2014; 15(10): 3550–3558. DOI: 10.1021/bm5007954.
29. Mao CS and Stavnezer J. Differential regulation of mouse germline Ig gamma 1 and epsilon promoters by IL-4 and CD40. *J Immunol* 2001; 167(3): 1522–1534. DOI: 10.4049/jimmunol.167.3.1522.
30. Nguyen HV, Mouly E, Chemin K, et al. The Ets-1 transcription factor is required for Stat1-mediated T-bet expression and IgG2a class switching in mouse B cells. *Blood* 2012; 119(18): 4174–4181. DOI: 10.1182/blood-2011-09-378182.
31. Jang YS, Seo GY, Lee JM, et al. Lactoferrin causes IgA and IgG2b isotype switching through betaglycan binding and activation of canonical TGF- β signaling. *Mucosal Immunol* 2015; 8(4): 906–917. DOI: 10.1038/mi.2014.121.
32. Grotzke JE and Cresswell P. Are ERAD components involved in cross-presentation? *Mol Immunol* 2015; 68(2 Pt A): 112–115. DOI: 10.1016/j.molimm.2015.05.002.
33. Zubareva AA, Shcherbinina TS, Varlamov VP, et al. Intracellular sorting of differently charged chitosan derivatives and chitosan-based nanoparticles. *Nanoscale* 2015; 7(17): 7942–7952. DOI: 10.1039/c5nr00327j.